Pure Appl. Chem., Vol. 80, No. 11, pp. 2499–2512, 2008.
doi:10.1351/pac200880112499

Control of deposition processes and structures of fibroin nanofilms by IR pulsed laser ablation*

Mamoru Senna[1,2,‡] and Sayuri Nakayama[2]

[1]Faculty of Science and Technology, Keio University, 3-14-1 Hiyoshi, Yokohama 223-8522, Japan; [2]Technofarm Axesz Co. Ltd., 3-45-4 Kamiishihara, Chofu, Tokyo 182-0035, Japan

Abstract: Control of structural and morphological features of silk fibroin (SF), one of the most popular and stable structural proteins, prepared by near infrared (1064 nm) pulsed laser deposition (PLD) are discussed, based mainly on the recent experimental studies made in the authors' laboratory. The small deposition rate and mingling of much larger units, called chunks or debris, are the main problems. The structure and properties of irradiation targets are highlighted, in an attempt to make the protein PLD technique affordable for practical purposes. Firm adhesion among fibroin powder particles is a straightforward way to avoid pull-out of the particles from the powder-consolidated target, being one of the main sources of debris. This alone cannot, however, satisfactorily increase the homogeneity of the nanostructures and increase the deposition rate. Finer control of the properties of grain-boundary in the target was therefore devised by using binders, including an autogenous one. A unique feature of the ablation mechanisms of fibroin was also discussed by taking account of the optical properties of fibroin, being transparent to a 1064 nm laser beam.

Keywords: thin films; fibroin; nanostructure; pulsed laser deposition; optical breakdown.

INTRODUCTION

Demands for engineered protein thin films are diverse and expanding. Regenerative medicine and modern biomedical treatments require smartly modified surface of the solids to be used as scaffolds or implants [1,2]. Coating solid surfaces for those articles with protein thin films is one of the promising techniques to fulfill the above-mentioned needs. To give bioaffinity to the substrate, uniform coverage irrespective of the substrate form is required with the firm adhesion retained after implantation into the animal body.

The objective of this article is to illustrate techniques to obtain a smooth, continuous, and homogeneous coating layer of proteins together with their scientific bases. We do not try to present a comprehensive review. Instead, we restrict ourselves to dry processing of fibroin films based on our own experimental results, while minimizing the part of overview of other techniques from the literature only for the purpose of indispensable comparison.

*Paper based on a presentation at the 3rd International Symposium on Novel Materials and Their Synthesis (NMS-III) and the 17th International Symposium on Fine Chemistry and Functional Polymers (FCFP-XVII), 17–21 October 2007, Shanghai, China. Other presentations are published in this issue, pp. 2231–2563.
‡Corresponding author: Fax: +81-42-483-4538; E-mail: senna@applc.keio.ac.jp

PROTEIN THIN FILMS

Protein films are used in many kinds of medical devices like biosensors and proteochips, to apply to antibody–antigen reaction, or surface modification of implants, to impart bioaffinitive property of protein. The required physical properties such as thickness, continuity, strength of adhesion, and morphology must be adaptable to the specification of the application. The preservation of higher-order structures throughout the film processing is generally appreciated. A number of studies have been reported from many points of view on the preservation or control of functional properties or higher-order structures. For instance, calixcrown was conjugated as a linker to protein to avoid inactivation [3]. A functional protein was conjugated in another case study in hydrogel and deposited on the substrate to preserve bioactivity of the protein after deposition [4]. These strategies can be applied to DNA or RNA chips as well. In standard film processing like dip- or spin-coating, it is needed to avoid agglomeration of various structural units during each step, i.e., dispersion of the protein in solution, adhesion to the substrate, drying, or storage.

Bovine serum albumin (BSA) thin films are easily prepared by depositing from a BSA solution on a flat substrate, while insoluble silk fibroin (SF) needs pretreatment to deposit via a sol-gel route. Starting with insoluble SF, we need to dissolve it with concentrated aqueous solution of $CaCl_2$, LiBr, or some enzymes. However, pretreatments take a long time, particularly to eliminate salts or enzymes. Furthermore, pretreatment is often accompanied by molecular degradation or reduction of the molecular weight [5]. Out of variations of film formation via a solution, electrospray deposition (ESD) has a unique feature. The method is based on the electrospray ionization, which is routinely used for mass spectroscopy [6]. Activity of enzymes after deposition is ascertained by alkaline phosphatase. Protein activity is better sustained by protective substances under appropriate humidity in the presence of disaccharides. ESD is also capable of fabricating fine porous films [7]. As a restriction, substrates should be electrically conductive. Patterning of protein films expands their application. Micropatterned membrane was made to examine biological structure–function relationship [8]. Soymilk skin can be patterned by various chemical stimuli [9].

SF from a silk worm, *Bombyx mori*, can be used as a favorable substrate of a biosensor [10–14], utilizing the amino acid residue of SF, Gly-Ala-Gly-Ala, favorable for sensing purposes. Liu et al. [10] introduced their structural advantages in their review, i.e., that its stability to most aqueous and organic solvents high tensile strength and elasticity. They reported its major merit as an enzyme immobilization without using cross-linking chemicals, which might deform and deactivate enzymes. An entrapment process is accomplished by configurational transition from silk I to silk II. Proteins are sometimes used with other bioaffinitive materials. SF–polyethylene glycol (PEG) composites were used for membrane of glucose biosensor [10].

DRY PROCESSING FOR PROTEIN FILMS

Pulsed laser deposition (PLD) is a good candidate of dry processing for protein thin film fabrication. PLD is particularly valuable for insoluble proteins like SF, since they do not allow any conventional deposition methods via a colloidal route without pretreatment. Irradiation of a 193-nm laser beam was examined on the frozen target of enzymes, to maintain the activity of the enzyme after deposition was examined [15,16]. Decomposition of proteins was suppressed by tuning the laser wavelength [17–20].

Tsuboi et al. [21–24] conducted serial studies in this field. They prepared SF thin film by PLD after chemically eliminating sericin. SF targets were irradiated by laser beam ranging from 248 to 532 nm. They observed dominance of the stable secondary structures of SF, β-sheet, in most cases. Their point was to add a laser absorber called photosensitizer. In their comprehensive achievement, they suggested photochemical mechanisms to be predominant with 248-nm beam, while less chemical decomposition occurred by 355-nm irradiation [21]. They mainly attributed the change in the surface morphology to the photon energy, in view of the relative role of photothermal and -chemical mechanisms.

We have achieved ablation and deposition of nanostructured SF by 1064-nm irradiation [25]. The threshold energy was empirically determined from the dependence of the film thickness as a function of laser fluence, shown in Fig. 1. The value, 1.7 J/cm^2, is appreciably higher than those with UV or visible laser beam, i.e., 0.4–0.5 J/cm^2. This suggests that the working mechanism of ablation and deposition in this study is significantly different from those in a series of works by Tsuboi et al., by using laser beam with much higher photon energy with or without photosensitizer, as mentioned above [21–24], or resonant infrared (RIR) PLD technique with a tunable laser to adapt specific wavelength of high absorbance [17–20].

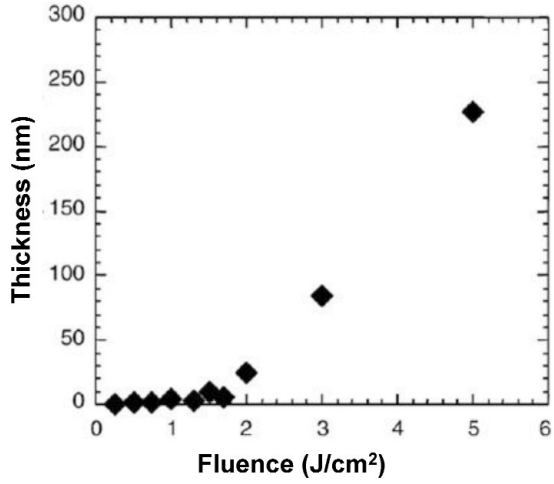

Fig. 1 Relationship between LF and film thickness, determined by QCM sensor, of the PLD films after 10 min irradiation.

The photon energy, 1.17 eV, of 1064-nm laser beam is much smaller than any covalent bond energies involved in SF used in this work, but significantly larger than that of hydrogen bonds, i.e., 0.10–0.40 eV [26,27]. Photochemical effect is, therefore, only possible, if at all, for the rupture of hydrogen bonds. The latter could happen under a negligibly small absorption coefficient shown in Fig. 2. In the early studies of ophthalmologic application of Q-switched 1064-nm laser beam with their

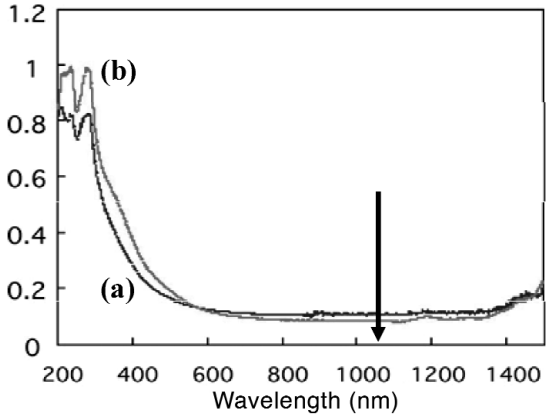

Fig. 2 UV–vis–NIR spectra of (a) untreated SF target and (b) granulated SF target with dissolved SF, which is treated by LiBr SF target. Samples were measured by diffusion reflectance.

nanosecond pulse duration, mechanisms with optical breakdown and subsequent cascade or avalanche ionization were well established [28–30], even when the source of the first free electron is controversial, including a possible contribution of impurities [31]. While multiphoton processes are unlikely in view of present nanosecond pulses, optical breakdown and associated cavitation and bubble development near the surface region are quite likely [32,33].

As shown in Fig. 3, the deposited film comprises island-like nanounits with their average projected size between 13–17 nm with scattered chunks up to 10 μm [25,34,35]. The authors have coined the former nanostructured unit as smallest protein unit (SPU). Increase in the fluence from 2 to 5 J/cm^2 increased the average size of the chunk. When the avalanche ionization goes on, the degraded area increases to increase the probability of chunk formation. As the chunk particles were blown off and collected, the particle size distribution was revealed to be similar to that of the intact SF particles to verify the pull-off of the SF particles from the consolidated target [35]. While the degradation of the target is probably associated with the rupture of hydrogen bonds among higher-order protein structures, its detailed feature is yet to be elucidated.

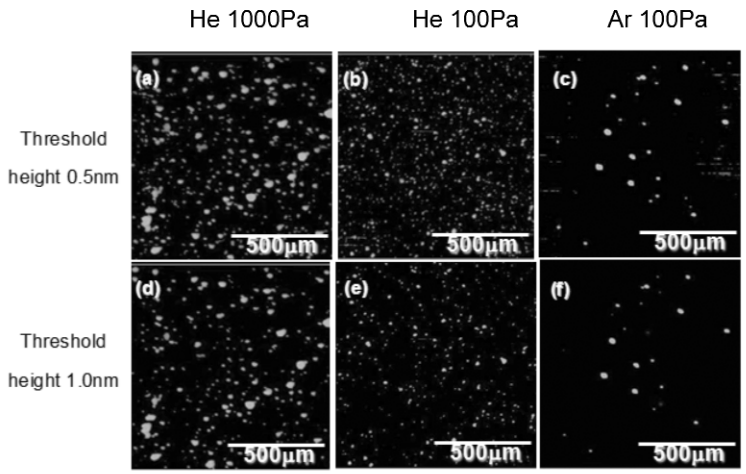

Background gas	Threshold height 0.5 nm	1.0 nm
He1000Pa	18.0	18.8
He100Pa	9.7	9.0
Ar100Pa	19.1	19.1

Fig. 3 AFM topological images of SF thin film deposited for 0.5 min at 2 J/cm^2 under varying background gas conditions. Background gas conditions for (a,d) are He 1000 Pa, (b,e) are He 100 Pa, and (c,f) are Ar 100 Pa.

Thus, near infrared (NIR) laser ablation brings about fairly uniform thin film of SF with its thickness as well as average size of the island-like SPU below 20 nm. We speculated the optical breakdown and subsequent avalanche ionization to be chiefly responsible for the ablation from an apparently transparent fibroin target. An apparent balance between rupture and reformation of hydrogen bonds seems to maintain the narrow size distribution of SPU. The merit of using NIR or IR laser to engineer the protein films is obvious, i.e., (i) to avoid breakage of protein main bonds and (ii) to use laser sources like Nd:YAG, which are relatively compact and inexpensive, and hence more friendly for practical application.

FACTORS INFLUENCING THE FILM QUALITY

The size of SPUs determined by atomic force microscopy (AFM) is not appreciably changed by deposition time or number of laser shots under the fixed fluence (2 J/cm^2) and background gas condition (He 100 Pa). In contrast, the change in the size distribution by the background gas conditions is quite significant [34]. As shown in Fig. 3 with an inset table, increasing the gas pressure from 100 to 1000 Pa

increased the unit size by a factor more than 2. By replacing background gas He with Ar, while keeping the pressure unchanged at 100 Pa, the average size of the SPU also increased significantly.

The effect of the background gas species was further examined by Fourier transform infrared–reflection adsorption spectroscopy (FTIR–RAS) for the SF thin films deposited on the Au-sputtered substrate after deposition by increasing gas pressure or changing gas species. FTIR–RAS spectra revealed that the relative contribution of random coil at around 1650 cm^{-1} became larger than that of β-sheet at around 1620 cm^{-1}. Growth of SPU during PLD with increasing the background gas pressure, and hence with increasing the number of gaseous molecules is generally explained by collision frequency and associated momentum exchange with the background gaseous molecules [36]. However, we also have to account for the specific properties of the protein species we deal with. The surface of the protein is rich in NH and C=O groups, capable of forming hydrogen bonds with neighboring species. Thus, the protein unit size is also associated with the interaction with other protein molecules or the substrate [37–41].

The state of plume was also quite different depending on the background gas condition. An increase in the pressure increases the volume of the plume zone. The plume was much larger with Ar than He when compared at the same pressure. We note that the first ionization potential of He is 24.59 eV, and that of Ar, 15.76 eV. Both are by far larger than that of the photon energy of IR laser, i.e., 1.17 eV of the 1064-nm beam. Direct ionization of the background gas is, therefore, to be excluded.

On the other hand, dissociation energy of hydrogen bond is well below the laser photon energy. When hydrogen bond rupture takes place, a part of intramolecular hydrogen bonds can change to either intra- or intermolecular ones to enhance the growth of SPU. We do not exclude similar hydrogen bond recombination leads to the formation of chunks, when it occurs after the establishment of nanoparticles. We do not exclude the possibility of role of coexisting cericin, whose ability of binding intrinsic fibroin units might be enhanced by partial disruption of its own hydrogen bonds by laser beam.

Possible destruction of protein units is extensively discussed in the interests of matrix-assisted laser desorption ionization with time-of-flight mass spectrometry (MALDI–TOFMS) [42–44]. Zehl et al. [45] showed with their sophisticated laser optical set-up, that with increasing laser fluence, the protein intact assembly is gradually replaced by nonassembled subunits with some apparent threshold. They found that disruption of noncovalent bonds takes place very rapidly at around the threshold fluence.

The apparent change of the plume size and eventually the plume color between He and Ar may thus be associated with the difference in the formation of ionized fragments of fibroin in the plume. The number of the ionic species increases with increasing the number and mass of gaseous species as stated above. At least phenomenologically, the growth of SPU is enhanced with an increasing amount of the ionized fragments indirectly estimated from the size of the plume. Since the ionization energy of the background gases is orders of magnitude larger than the photon energy of the laser, it is more likely that the effects of background gas is predominantly associated with their physical properties. Thus, the unique feasibility of designing microstructures of the fibroin thin films deposited by PLD is well expected by controlling the background gas condition.

FORMATION AND ELIMINATION OF DEBRIS

Debris or chunks commingled in a majority of the areal fraction of the deposition are broadly classified into two, i.e., simple pull-out of the particulates comprising the target made from ingredient powders either by compression–consolidation or by sintering; and from droplets formed by partial or local liquefaction. We therefore systematically examined the occurrence of debris.

Debris up to 50 μm was observed on the SF film deposited at 2 J/cm^2, under the optical microscope. Local distribution of the deposition was examined by the set-up shown in Fig. 4. As shown in Fig. 5, the largest amount of chunks was deposited at the central position (0,0) than other substrates in a horizontal position, while much fewer chunks are observed on the substrate in a vertical position, v1. When the same film was observed under AFM, densely packed SPUs were recognized in the majority

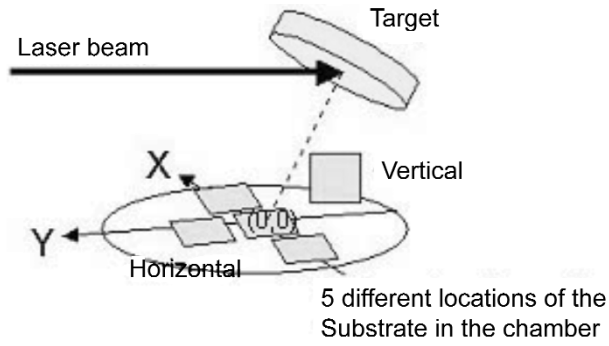

Fig. 4 Scheme of the location of the substrates in the PLD chamber.

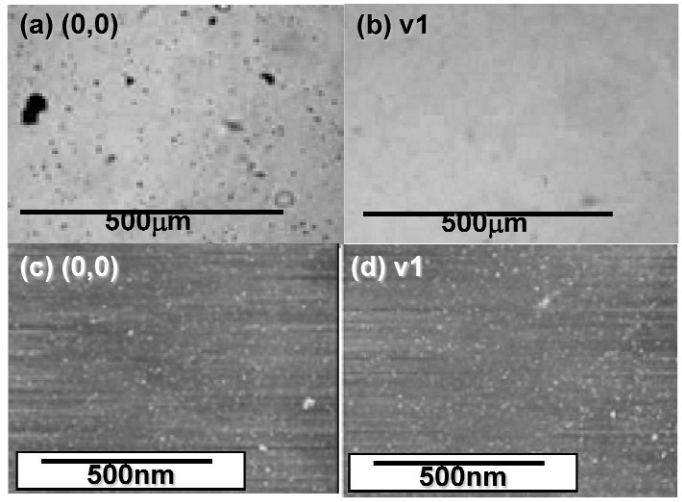

Fig. 5 Difference of the occurrence of large particulate units in the PLD film, prepared at 2 J/cm^2 for 0.5 min, depending on the location of the substrates observed under the optical microscope (a,b). (a) (0,0), horizontal and (b) vertical. (c,d) are AFM images corresponding to the optical micrographs of (a) and (b), respectively.

of the substrate areas. Note that the difference in the values of the root-mean-square surface roughness, R_{rms}, was insignificant, i.e., 0.394 and 0.386 nm, in the view area of 1×1 μm for the position of (0,0) and v1, respectively.

Elimination of debris was realized by gaseous blow-off (GBO) treatment on the films prepared under the same condition, i.e., at 2 J/cm^2 for 0.5 min at the linear gas flow rate of 580 m s^{-1}, being maximum in a series of experiments. Elimination of chunks by GBO treatment was observed by comparing scanning electron micrographs (SEMs) before and after GBO. The values of R_{rms} determined by the laser microscope before and after GBO were 0.34 and 0.30 μm, so that the change in R_{rms} seems insignificant either, as shown in Fig. 6. Note that extremely large chunks often remain unblown. Particles between 1 and 10 μm, correspond to the size of the intact SF powder, so that it is clear that the main source of the debris is the SF particles themselves pulled out of the target.

While debris particles are eliminated by post-treatments like GBO described above, it is obviously smarter when the occurrence of debris is suppressed. Since we observed that the main source of the debris is the pull-out of the particles from the target, harder consolidation of the target is the next effort for more homogeneous films.

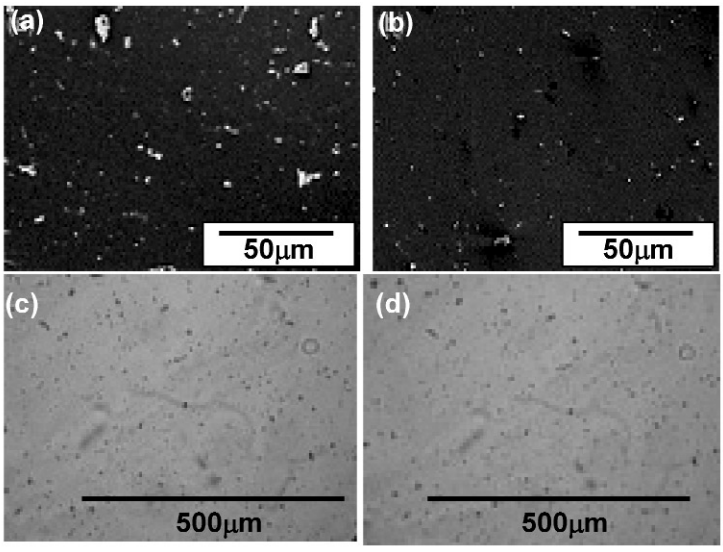

Fig. 6 (a,b) SEMs of the PLD film deposited at 2 J/cm^2 for 0.5 min; (a) as deposited and (b) after GBO treatment for 5 min. (c,d) OM images for the same samples as (a,b).

CONTROL OF TARGET STRUCTURE

Increase in the target hardness

We first attempted to increase the adhesion among particulate units in the target to avoid pull-out due to degradation during laser irradiation. This does not sacrifice the throughput of deposition. On the contrary, an increase in the efficiency of PLD is expected due to higher probability of optical breakdown with appropriate additives, which produces free electrons during laser irradiation. This, in turn, enables us to trigger an electron avalanche. More specifically, a significant reduction of the amount of larger units was achieved by adding a small amount of sticky aqueous sol of cellulose derivatives to the SF powder to make a harder target.

The effects of binder, hydroxypropyl methylcellulose (HPMC), were first examined for better consolidation of the targets, in an attempt to avoid debris and to obtain smoother, more homogeneous nanostructured fibroin films. Granules were prepared by extrusion via a sieve after adding an aqueous solution of HPMC as a binder. After drying the granules in air, they were confined in the cylindrical mold and compressed to obtain the targets SF–HPMC with the content of HPMC up to 5 wt %.

AFM and SEM images of the deposited film are shown in Fig. 7. The fraction of finer SPUs increased with increasing binder concentration. The average size of SPU and deposition rate of debris were decreased by 17 and 33 %, respectively, by adding 5 % HPMC. It is also important to note that the variation coefficient of the particle size decreased by a factor 3~6 by the addition of the binder. These results demonstrate that the use of a binder brings about finer and more uniform nanostructured film.

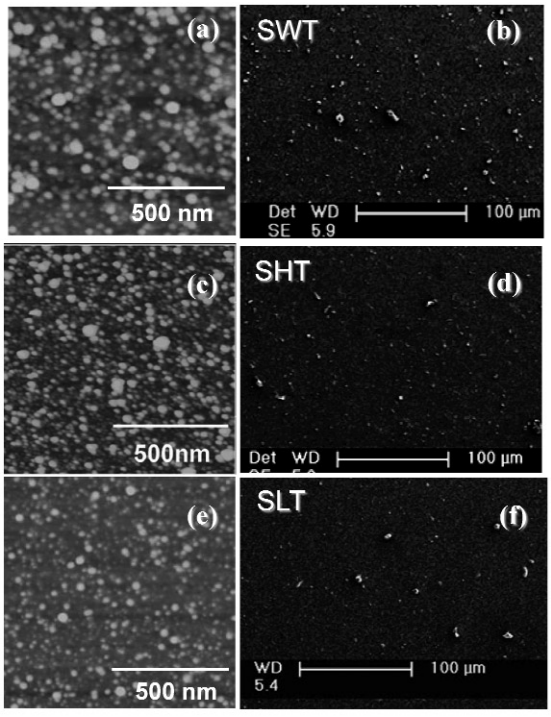

Fig. 7 (a,c,e) AFM and (b,d,f) SEM images of SF films deposited by PLD at 5 J/cm^2 for 2 min in He 100 Pa. Target was prepared by compressing of granule with (a,b) water (SWT), (c,d) 5 % HPMC (SHT), (e,f) swollen SF by LiBr (SLT).

From low-magnification SEM image, the fraction of debris was determined as a fraction of the area A_d occupied by the particles larger than the resolution limit of the image, 2 µm. As shown in Table 1, a decrease in the debris fraction by using HPMC binder is significant.

Table 1 Average size of nanoparticles, coating rate of debris of the films, and Vickers hardness of the SF targets prepared by different binders, i.e., water, 5 % HPMC, or liquefied SF with 5 % LiBr.

		SLT	SWT	SHT
Morphologies nanofilms by AFM	Average particle size [nm]	18.4 ± 7.1	25.8 ± 3.2	22.2 ± 0.7
	D_{50} of nanoparticles [nm]	16.0	28.0	14.8
	R_{rms} [m]	1.84	2.76	3.19
Percent area of debris by SEM	D_{50} of debris [mm]	1.9	2.3	3.1
	A_d [%]	1.2	2.5	1.6
Thickness by QCM	Depostion rate [nm/min]	20.9	8.3	8.2
Vickers hardness of the target	[-]	82.4 ± 10.4	32.7 ± 8.2	86.3 ± 29.3
	Variation coefficient	0.13	0.25	0.34

The Vickers microhardness increased with increasing the HPMC concentration in the binder, as also shown in Table 1. This might explain the decrease in the chunk fraction by suppressing the pull-out of the SF particles right from the target. The surface structure shown in Fig. 8 demonstrates the suppression of the particle pull-out. However, a simultaneous change in the nanostructure, the increase in the homogeneity of SPUs in particular, cannot be the direct consequence of increase in the interparticle cohesion. Homogenization of the film by the introduction of binder should rather be interpreted in the light of the mechanisms of the deposition.

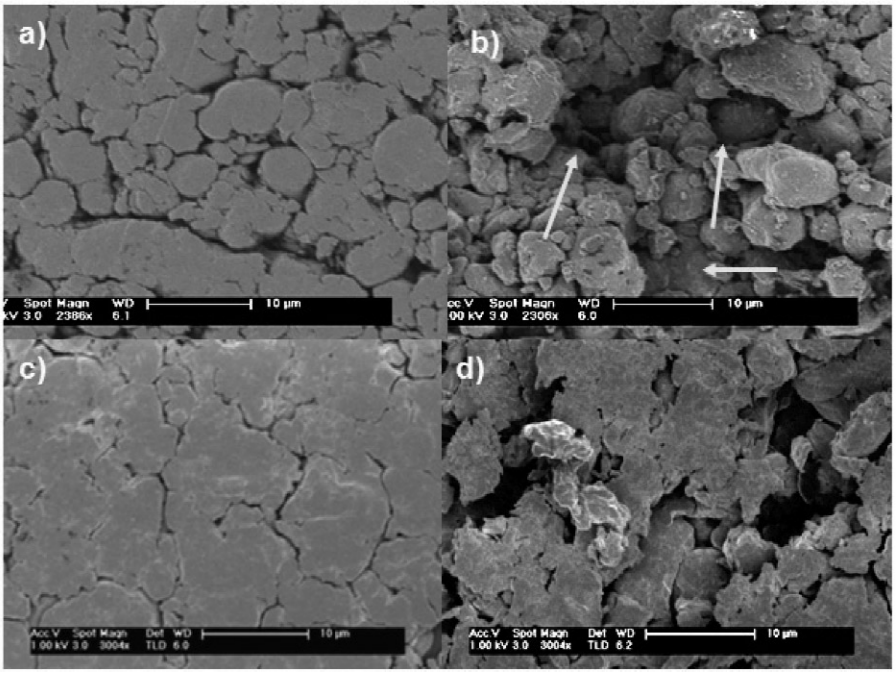

Fig. 8 SEMs of (a,b) SFH0 and (c,d) SFH5 target. (a,c) before, and (b,d) after irradiation of 1064-nm beam at 5 J/cm^2.

Targets with autogenous binder

We have further tried to improve the target not only to avoid debris formation but also to obtain more homogeneous fibroin film and, more importantly, at a higher deposition rate. For these purposes, liquefied fibroin was adopted as an autogenous binder.

The outer shell of the natural cocoon was cut into pieces of 5×5 mm and boiled successively in 0.5 % Marseille soap solution, twice in 0.3 % aqueous solution of Na_2CO_3, and finally in deionized water to eliminate silk sericin. After each boiling procedure, solutions were separated by centrifugation and decantation. After drying at room temperature for 24 h, degummed SF (DSF) was obtained. Subsequently, 5.0 g LiBr powder was added to 2.0 g of DSF. After these procedures, highly viscous and homogeneous fibroin paste was obtained to serve as an autogenous binder. A target was obtained by using liquid SF as an autogenous binder and extruding through a sieve mesh with its opening 840 μm to obtain granules after drying at 50 °C. The granules were then compressed uniaxially to obtain an all-fibroin SF-liquid target (SLT). For comparison, reference targets were prepared by replacing the autogenous binder either with water (SWT), or with 0.10 g of HPMC (SHT).

Micrographs obtained from AFM for the smallest particle units in the nanometer range (SPUs), and SEM for debris particles of SLT and SWT are shown in Figs. 9A and 9B, respectively. The cumu-

lative size distribution of SPUs in the films prepared from SWT, SLT, and SHT was then evaluated. As shown in Fig. 10, size distribution was significantly different between the films by using SLT and SWT. The numerical values are summarized in Table 1. The median particle size, D_{50}, of SPU was 16 nm for the film from SLT target. This is significantly smaller than those from SWT target, 28 nm. Note that the resolution of the AFM image at this view was 3.9 nm/pixel, so that the difference in D_{50} is definitely significant.

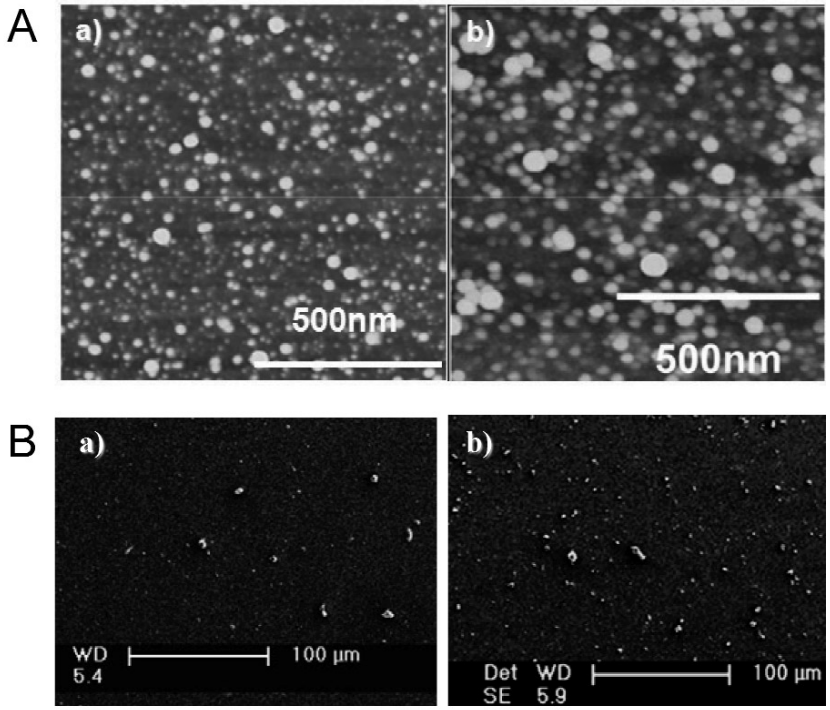

Fig. 9 (A) AFM and (B) SEM images of (a) SLT and (b) SWT film deposited by PLD at 5 J/cm^2 for 2 min.

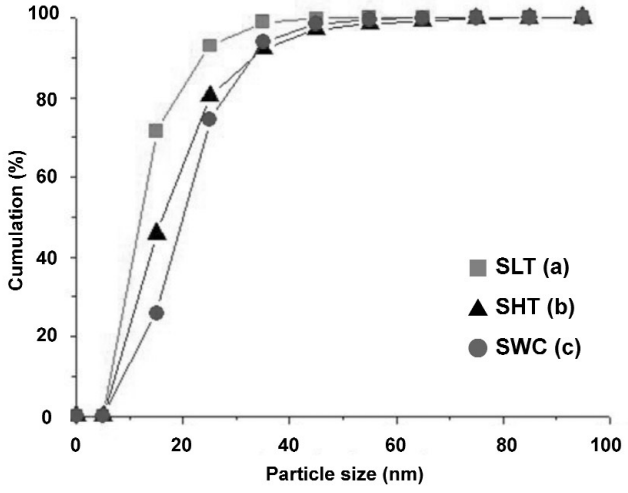

Fig. 10 Cumulative particle size distribution of SPUs in the films prepared from (a) SLT, (b) SWT, and (c) SHT film evaluated from Fig. 9A.

Cumulative size distribution curves of the debris, mainly due to direct pull-out of SF particles from the target, were evaluated from Fig. 9B and shown in Fig. 11. The difference in the median value, D_{50}, of debris particle size in the films from SLT and SWT targets, given in Table 1, is within a pixel size, 1.2 μm, and hence regarded as insignificant.

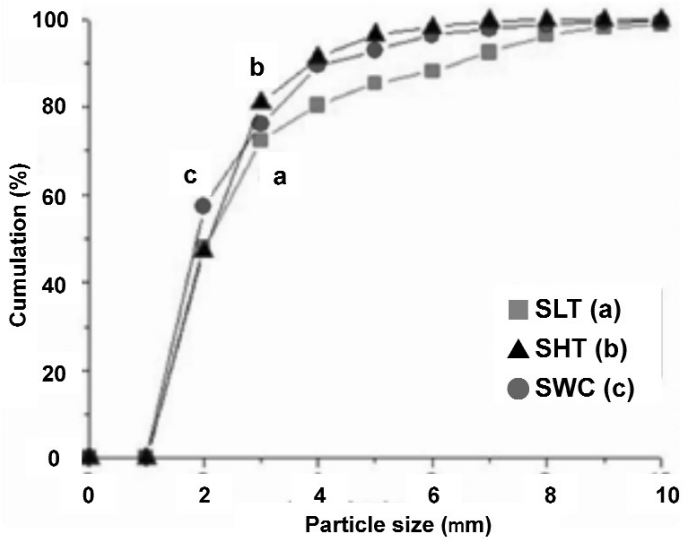

Fig. 11 Cumulative particle size distribution of the debris of (a) SLT, (b) SWT, and (c) SHT film, evaluated from Fig. 9B.

From the image analysis, the percent area, A_d, occupied by the particles more than twice as large as the pixel size was determined. The value A_d was decreased to 48 % of those from the SWT target, or to 64 % of those from the SHT target. The deposition amount of debris was thus reduced by granulation with binders used for the purpose of better consolidation of the targets.

The average relative hardness of the SLT target is larger by a factor of 2.5, compared with SWT. Likewise, the relative hardness increased by a factor of 2.6 in the case of the SHT target. The variation coefficient of micro-Vickers hardness of SLT decreased to 52 % compared to SWT, while it increased by a factor of 1.4 in the case of SHT. This indicates that the autogenous binder makes the target more homogeneous than with non-autogenous ones. These results imply that not only hardness but also homogeneity of the target can be regulated by the choice of the binder. It is obvious that harder and more homogeneous targets are beneficial for uniform PLD film with less debris.

The rate of deposition of SLT film determined by quartz crystal microbalance (QCM), shown in Fig. 12, was larger than SWT. We previously observed an apparent increase in the deposition rate with simultaneous increase of the debris fraction [46]. This is obviously attributed to the heavier particles in the debris and does not make sense from the viewpoint of film quality. In the present case with an autogenous binder, in contrast, decrease in the debris percent and increase in the deposition rate occur simultaneously. Therefore, the net increase in the deposition rate of nanostructured portion is much larger than the apparent increase seen in Fig. 12.

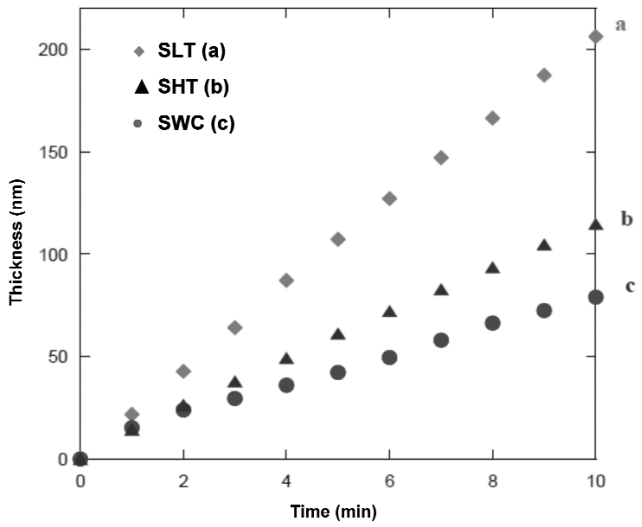

Fig. 12 Relationship between deposition time and film thickness, determined by QCM sensor, of (a) SLT, (b) SWT, and (c) SHT film deposited by PLD at 5 J/cm^2.

SUMMARY AND CONCLUDING REMARKS

Homogeneous deposition of nanostructured fibroin thin film by NIR PLD is quite possible. The secondary structure of fibroin, being β-sheet in a stable state, could mostly be preserved as far as the laser fluence is kept to be slightly above the threshold value. Consolidation of irradiation targets is one of key issues to reduce chunks. Liquefied fibroin serves as a good binder for targets and may have affected avalanche mechanisms positively. The main mechanism, optical breakdown, is, however, not yet fully elucidated. While fine structure of the irradiation target is considered to be preferable for stable plume, we have yet to elucidate the mechanisms and the technical methodology standing upon the sound scientific basis.

ACKNOWLEDGMENTS

The authors thank Mr. T. Sato and Ms. R. Nozaki for their cooperation in experimental studies. This work was partly supported by Grant-in-Aid for 21st Century COE program "KEIO Life Conjugate Chemistry" from the Ministry of Education, Culture, Sports, Science, and Technology, Japan. The authors thank suppliers for materials used in the experiments, i.e., Idemitsu Petrochemicals for SF powders, Komatsu Electronic Metals for Si wafers, National Institute of Agrobiological Science for cocoon samples, Lion Corp. for Marseille soap, and Shinetsu Chemicals for HPMC.

REFERENCES

1. I. Georgakoudi, I. Tsai, C. Greiner, C. Wong, J. DeFelice, D. Kaplan. *Opt. Express* **15**, 1043 (2007).
2. K. Cai, Y. Hu, K. D. Jandt. *J. Biomed. Mater. Res., A* **82**, 927 (2007).
3. Y. Lee, E. K. Lee, Y. W. Cho, T. Matsui, I. Kang, T. Kim, M. H. Han. *Proteomics* **3**, 2289 (2003).
4. D. Guschin, G. Yershov, A. Zaslavsky, A. Gemmell, V. Shick, D. Proudnikov, P. Arenkov, A. Mirzabekov. *Anal. Biochem.* **250**, 203 (1997).
5. M. Tsukada, Y. Gotouh, M. Nagura, N. Minoura, N. Kasai, G. Freddi. *J. Polym. Sci., Part B: Polym. Phys.* **32**, 961 (1994).

6. V. N. Morozov, T. Y. Morozova. *Anal. Chem*. **71**, 1415 (1999).
7. I. Uematsu, H. Matsumoto, K. Morota, M. Minagawa, A. Tanioka, Y. Yamagata, K. Inoue. *J. Colloid Interface Sci*. **269**, 336 (2004).
8. J. Shaikh Mohammed, M. A. DeCoster, M. J. McShane. *Biomacromolecules* **5**, 1745 (2004).
9. S. Nakata, A. Terada, A. Yamada, M. Denda, Y. Mori. *Mater. Sci. Eng., C* **27**, 633 (2007).
10. Y. Liu, T. Yu. *J. M. S. Rev. Macromol. Chem. Phys*. *C* **37**, 459 (1997).
11. Y. Tu, Z. Fu, H. Chen. *Sens. Actuators, B* **80**, 101 (2001).
12. H. Liu, H. Deng, K. Sun, D. Qi, J. Deng, Y. Liu, T. Yu. *Fresenius' J. Anal. Chem*. **357**, 812 (1997).
13. A. P. Valaitis, A. R. Brousseau, L. Masson. *Insect Biochem. Mol. Biol*. **27**, 529 (1997).
14. Y. Q. Zhang. *Biotechnol. Adv*. **16**, 961 (1998).
15. B. R. Ringeisen, J. Callahan, P. K. Wu, A. Pique, B. Spargo, R. A. McGill, M. Bucaro, H. Kim, D. M. Bubb, D. B. Chrisey. *Langmuir* **17**, 3472 (2001).
16. P. K. Wu, B. R. Ringeisen. *Rev. Sci. Instrum.* **74**, 2546 (2003).
17. D. M. Bubb, J. S. Horwitz, J. H. Callahan, R. A. McGill, E. J. Houser, D. B. Chrisey, M. R. Papantonakkis, A. Vertes. *J. Vac. Sci. Technol.*, *A* **19**, 2698 (2001).
18. D. M. Bubb, J. S. Horwitz, R. A. McGill, D. B. Chrisey, M. R. Papantonakkis, R. F. Haglund Jr., B. Toftmann. *Appl. Phys. Lett.* **79**, 2849 (2001).
19. D. M. Bubb, B. Toftmann, R. F. Haglund Jr., J. S. Horwitz, M. R. Papantonakkis, R. A. McGill, P. W. Wu, D. B. Chrisey. *Appl. Phys. A* **74**, 123 (2002).
20. B. Toftmann, M. R. Papantonakkis, R. C. Y. Auyeung, W. Kim, S. M. O'Malley, D. M. Bubb, J. S. Horwitz, J. Schou, P. M. Johansen, R. F. Haglund. *Thin Solid Films* **453–454**, 177 (2004).
21. Y. Tsuboi, M. Goto, A. Itaya. *Chem. Lett.* 521 (1998).
22. Y. Tsuboi, M. Goto, A. Itaya. *J. Appl. Phys*. **89**, 7917 (2001).
23. Y. Tsuboi, T. Ikejiri, S. Shiga, K. Yamada, A. Itaya. *Appl. Phys. A* **73**, 637 (2001).
24. Y. Tsuboi, H. Adachi, K. Yamada, H. Miyasaka, A. Itaya. *Jpn. J. Appl. Phys*. **41**, 4772 (2002).
25. S. Nakayama, S. Nagare, M. Senna. *Thin Solid Films* **515**, 2582 (2006).
26. D. Katagiri, T. Tsuchiya, M. Tsuda, M. Hata, T. Hoshino. *J. Phys. Chem. B* **106**, 9151 (2002).
27. S. Y. Sheu, D. Y. Yang, H. L. Selzie, E. W. Schlag. *Proc. Natl. Acad. Sci. USA* **100**, 12683 (2003).
28. A. Vogel, V. Venugopalan. *Chem. Rev*. **103**, 577 (2003).
29. A. Vogel, M. R. C. Capon, M. N. A. Vogel, R. Birngruber. *Investig. Ophthalmol. Vis. Sci*. **35**, 3032 (1994).
30. C. L. Arnold, A. Heisterkamp, W. Ertmer, H. Lubatschowski. *Appl. Phys. B* **80**, 247 (2005).
31. J. Noack, A. Vogel. *IEEE J. Quant. Electron*. **35**, 1156 (1999).
32. H. Lubatschowski, A. Heisterkamp. *Top. Appl. Phys*. **96**, 91 (2004).
33. G. Freedi, P. Monti, M. Nagura, Y. Gotoh, M. Tsukada. *J. Polym. Sci., Part B: Polym. Phys.* **35**, 841 (1997).
34. S. Nakayama, M. Senna. *J. Phys. Conf. Ser*. **59**, 92 (2007).
35. S. Nakayama, M. Senna. *J. Phys. Conf. Ser*. **59**, 96 (2007).
36. Y. Yamada, T. Orii, I. Umezu, S. Takeyma, T. Yoshida. *Jpn J. Appl. Phys*. **35**, 1361 (1996).
37. M. I. Janssen, M. B. M. van Leeuwen, T. G. van Kooten, J. de Vries, L. Diikhuizen, H. A. B. Wosten. *Biomaterials* **25**, 2731 (2004).
38. M. Otto, B. Wahn, C. J. Kirkpatrick. *J. Mater. Sci. Mater. Med.* **14**, 263 (2003).
39. R. E. Unger, K. Peters, M. Wolf, A. Motta, C. Migliaresi, C. Kirkpatrick. *J. Biomater.* **25**, 5137 (2004).
40. B. M. Min, L. Jeong, T. S. Nam, J. M. Kim, J. Y. Kim, W. H. Park. *Int. J. Biol. Macromol.* **34**, 281 (2004).
41. M. A. Hernandez-Perez, C. Garapon, C. Champeaux, A. W. Coleman, P. Shahgaldian, J. Mugnier. *Appl. Phys. A* **79**, 1473 (2004).
42. K. Dreiseverd. *Chem. Rev*. **103**, 395 (2003).
43. M. Karas, R. Kruger. *Chem. Rev*. **103**, 427 (2003).

44. R. Knochenmuss, R. Zenobi. *Chem. Rev*. **103**, 441 (2003).
45. M. Zehl, G. Allmaier. *Anal. Chem*. **77**, 103 (2005).
46. S. Nakayama, T. Sato, M. Senna. *J. Mater. Sci. Lett*. **42**, 4120 (2007).